2021 ICRACOS
INTERNATIONAL CONFERENCE ON RESEARCH AND ACADEMIC COMMUNITY SERVICES

**2021 3rd International Conference on Research and Academic Community Services (ICRACOS)**
http://icracos.lppm.unesa.ac.id

No. : 46719/UN38.I/DL.01.02/2021

UNESA

# CERTIFICATE

This certificate awarded to

## Dany Iman Santoso

as

Presenter Article entitle

**Investigation of the droplet properties along their trajectory in cooling tower**

**at 2021 3rd International Conference on Research and Academic Community Services (ICRACOS) with theme " Sustainable Innovation in Research and Community Services for Better Quality of Life towards Society 5".**

**Surabaya, 9th - 10th October 2021**

**Vice Rector for Academic Affairs,**

**Prof. Dr. Bambang Yulianto, M.Pd.**

**Conference Chair,**

**Dr. Nurhayati, S.T., M.T.**

IEEE INDONESIA SECTION
MTT-S IEEE MTT/AP CHAPTER INDONESIA
UNESA Universitas Negeri Surabaya

# I. Investigation of the Droplet Properties Along Their Trajectory in the Cooling Tower


Dany Iman Santoso
*Dept. of Mechanical Engineering*
*Universitas Negeri Surabaya*
Surabaya, Indonesia
danysantoso@unesa.ac.id

I Wayan Susila
*Dept. of Mechanical Engineering*
*Universitas Negeri Surabaya*
Surabaya, Indonesia
wayansusila@unesa.ac.id

Dewanto
*Dept. of Mechanical Engineering*
*Universitas Negeri Surabaya*
Surabaya, Indonesia
dewanto@unesa.ac.id

Yunus
*Dept. of Mechanical Engineering*
*Universitas Negeri Surabaya*
Surabaya, Indonesia
yunus@unesa.ac.id

Akhmad Hafizh Ainur Rasyid
*Dept. of Mechanical Engineering*
*Universitas Negeri Surabaya*
Surabaya, Indonesia
akhmadrasyid@unesa.ac.id

Rachmad Syarifudin Hidayatullah
*Dept. of Mechanical Engineering*
*Universitas Negeri Surabaya*
Surabaya, Indonesia
rachmadhidayatullah@unesa.ac.id



***Abstract*—Water capacity is the most crucial thing in the evaporation process in the cooling tower. Therefore, at the initial setting, the manufacturer limited the load or the point of equilibrium so that no drifting or mass transfer occurs during the process. Mass transfer means that the cooling tower was experiencing a water deficit. This experiment used a mechanical draft wet cooling tower (MDWCT) with varying water capacities between 0.5 – 18 litters per minute (Lpm). This study changed air capacity also through variations in fan rotation between 300 – 1500 rpm. In the previous calculation, the value of 6 Lpm was obtained as the equilibrium capacity. Mathematical modelling based on Reynolds Averaged Navier-Stokes (RANS) was applied to simulate the interactions. It presented heat and mass transfer by mass and temperature charts, respectively, and their reductions. For low capacity (0.5 Lpm), water undergoes mass transfer, as proven by the mass flow reduction graph value of $10^{-8}$ kg/(m.s). Meanwhile, for high capacity (18 Lpm), water experiences heat transfer as evidenced by the temperature difference graph value of 11°C.**



***Keywords—water capacity, evaporation process, point of equilibrium, drifting process, heat and mass transfer.***


## II. Introduction

Spraying process, it converts the liquid into droplets of various sizes (radii) and includes polydispersed multiphase flows [1]. And the complexity of this process is that the formation of the spray by an atomizer involves many mechanisms [2]. One of the modifications in the spraying process was to include air induction at the nozzles. Sprayers that used air-induced nozzles can reduce drift problems by producing larger droplets than similar nozzles without air induction [3].

Behind the complexity of the atomization process, droplets store high latent heat during the evaporation process so that it can be used in many applications such as cooling towers [4]. The multi droplet approach is more feasible to use than the single droplet because it is closer to the experimental results [5]. The widely used model in droplet heating, both evaporating and non-evaporating, is a model that assumes an infinitely large liquid thermal conductivity [6]. It means that the droplets spend the heat absorbed to raise the droplet temperature. Most of these models assume that the droplets are spherical [7].

There are two distinguished stages of droplet heating [8]. The first is the stage where the temperature increases rapidly throughout the droplet and, the second is the stage where the temperature increases slowly to become quasi-steady [8–9]. During heating, heat and mass transfer occurs between the wet surface and dry air [9–10]. Also, the mass transfer interactions between gases and liquids may depend on the physical properties of the liquid or gas, process parameters, and system geometry [11].

The results obtained by Santoso et al. [12] were that low water capacity (0.5 Lpm) produced large droplet diameters ($10^{-3.6}$ m), and high capacity (18 Lpm) showed small droplet diameters ($10^{-4.6}$ m) for 300 rpm fan rotation in the spray zone. The higher the volume rate, the smaller the diameter. This statement also applies to higher fan rotation. This study examines the effect of changing droplet diameter on other properties along the trajectory that cause heat and mass transfer. The cooling tower scheme and the parameters used are presented in Fig. 1 and Table 1, respectively.

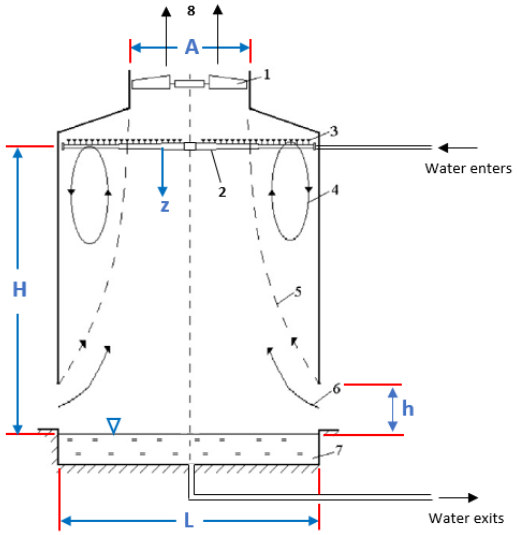


Fig. 1. The scheme of the cooling tower: (1) The suction fan, (2) The pipeline, (3) The nozzles, (4) The stagnation zone, (5) The edge of the stagnation zone, (6) The air enters, (7) The water collector, (8) The air exit.

Fig. 1 shows how the working fluid interaction pattern takes place. Hot water entered the cooling tower through the pipe above and was sprayed through the nozzle holes on the pipe wall. The hot water then fell to the bottom of the cooling tower due to gravity. At the same time, the air around the cooling tower was sucked into it. Air enters the cooling tower through the holes in the walls. The air moves up because of the fan suction above the cooling tower. The interaction


DOI: 10.1109/ICRACOS53680.2021.9702033 ©2022 IEEE

between hot water and cold air occurs along with the cooling tower.

TABLE I. THE COOLING TOWER PARAMETERS

| No. | Parameters | | |
|---|---|---|---|
| | ***Dimensions*** | ***Value*** | ***Units*** |
| 1 | Tower height (H) | 0.56 | m |
| 2 | Base diameter (L) | 0.65 | m |
| 3 | Roof area (A) | 0.032 | $m^2$ |
| 4 | Window height (h) | 0.20 | m |
| 5 | Nozzle diameter ($d_n$) | 0.001 | m |
| 6 | Water capacity ($Q_w$) | 0.5–18[a] | Lpm |
| 7 | Fan rotation ($n_f$) | 300–1500[a] | rpm |

[a.] Measurements are in steady state condition

## III. METHODS

### A. Numerical Model

This study divided the cooling tower height into three zones of equal length. The three zones are spray, fill, and rain. It was done because the elevation of the cooling tower was relatively short as a prototype. For the fill zone, packing with an S-wave of 1.25 m was used. Besides, the boundary conditions of ambient pressure and temperature were 1 atm and 30° Celsius, respectively. The wind speed around the test site was almost non-existent because the experiment was done indoors. So air movement was only due to the suction from the fan that it was placed on the roof of the cooling tower.

The cooling tower in this study was a counterflow type and the working fluid used was liquid water and air. Because there were two different fluid phases, stochastic analysis can be used. This study considered the second one as a continuous phase. It figured out using the Euler framework. Meanwhile, another was counted as a discrete phase. It worked out with the Lagrange framework. The following are the governing equations for both analyzes.

### B. Governing for Air Flow

Reynolds Averaged Navier-Stokes equation for steady-state condition models the turbulent flow of continuous phase which is a compressible flow [13–17] as

$$\nabla \cdot \left(\rho \vec{u} \varphi - \Gamma_\varphi \nabla \varphi\right) = S_{\varphi i} + S_\varphi \tag{1}$$

These are the air density $\rho$, the air velocity components $u_x$, $u_y$ and $u_z$, the dependent variables for air flow $\varphi$ that gives the value of 1 for the equation, the diffusion coefficient for air variable $\Gamma_\varphi$, also $S_{\varphi i}$ and $S_\varphi$ are the internal source and source terms, respectively. To simplify calculations, air was considered as ideal gas and water was considered as water vapor.

Air density depends on the temperature where it is located. The following equation calculates air density $\rho$ [17, 18] as

$$\rho = p_a / \left(\frac{R}{M_w} T\right) \tag{2}$$

These are the ambient pressure $p_a$, the air molecular weight $M_w$, the universal gas constant $R$, and the air temperature $T$.

Based on continuity principle for the continuous phase [19], the velocity of air on the z-axis $u_z$ is obtained as

$$u_z = Q/(\rho L^2) \tag{3}$$

These are the air capacity $Q$ that is yielded from fan rotation $n_f$ and the bottom side of the tower $L$.

### C. Governing for Water Flow

The droplet moves downward so that gravity dominates its movement. From the momentum equation for incompressible flow [18, 20] obtained

$$\frac{du_{wz}}{d(-z)} = \frac{(\rho_w - \rho)g}{\rho_w u_{wz}} - \frac{f_z}{m_w u_{wz}} \tag{4}$$

These are the z-axis velocity of a droplet $u_{wz} = Q_w/A_n$ that is given from the water capacity $Q_w$ and the nozzle cross-section area $A_n$, the gravitational acceleration $g$, the water droplet mass $m_w$, and the water droplet resistance force $f_z$ caused by the counter flow of air as

$$f_z = C_d Re_d \frac{\pi d \mu_w}{8} u_{wz} \tag{5}$$

This is the dynamic viscosity of water $\mu_w$.

For the drag coefficient $C_d$ [21], the droplet Reynolds number $Re_d$ [22], and the droplet diameter $d$ [23] are given in the Eq. (6), Eq. (7), and Eq. (8), respectively.

$$C_d = \frac{24}{Re_d}(1 + 0.15 Re_d^{0.687}) + \frac{0.42}{1 + 4.25 \times 10^4 Re_d^{-1.16}} \tag{6}$$

$$Re_d = \frac{d(u_{wz} - u_z)}{\nu_w} \tag{7}$$

$$d = Cb\alpha^{-1/6} We^{-1/3} \tag{8}$$

These are the kinematic viscosity of water $\nu_w$, the dimensionless constant $C$ that is $C = 1.95$, the characteristic length $b$ that is $b^2 \sim A_n$, the density ratio $\alpha$ that is $\alpha = \rho/\rho_w$, and the Weber number $We$ [23, 24] that is

$$We = \rho_w u_{wz}^2 b / \sigma_w \tag{9}$$

where $\sigma_w$ is the surface tension of water.

Three zones, from the roof to bottom of the cooling tower, are spray, fill, and rain. The first and third usually have the same characteristics, so the modeling of these uses the same approach.

### D. Interaction between air and water in spray and rain

The interaction between water and air molecules is depicted in Fig. 2. In the Lagrange framework for the discrete phase, the coefficient of heat or mass transfer from the surface of the droplet is calculated from the correlation of Nusselt and Sherwood numbers [13–14, 17–18] as Eq. (10) and Eq. (11), respectively.

$$Nu = \frac{hd}{k_\infty} = 2.0 + 0.6 Re_d^{1/2} Pr^{1/3} \tag{10}$$

$$Sh = \frac{h_m d}{D_m} = 2.0 + 0.6 Re_d^{1/2} Sc^{1/3} \tag{11}$$

These are the Prandtl number of air *Pr*, the Schmidt number of air *Sc*, the thermal conductivity of air $k_\infty$, the water diffusion coefficient in air $D_m$, the coefficient of heat transfer *h*, and the coefficient of mass transfer $h_m$.

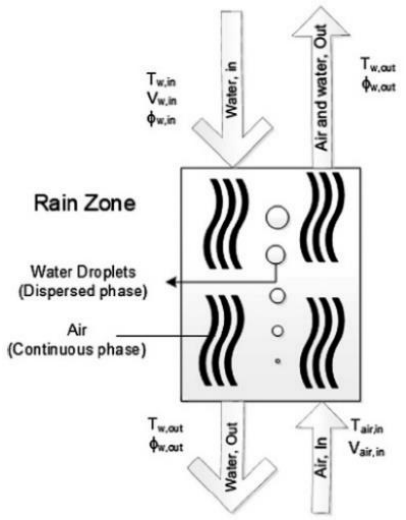


Fig. 2. The water droplet flow model falls in the forced air counterflow stream.

Then the number of the droplet per unit volume $N_d$ and the surface area of the droplet $A_d$ are as Eq. (12) and Eq. (13), respectively.

$$N_d = \frac{6Q_w}{u_{wz}\pi d^3} \tag{12}$$

$$A_d = \pi d^2 \tag{13}$$

Combining Eq. (10) until Eq. (13) generates volumetric heat $K_h$ and mass $K_a$ transfer coefficient [17, 18] as follows in Equation (14) and Equation (15), respectively.

$$K_h = N_d A_d h \tag{14}$$

$$K_a = N_d A_d h_m \tag{15}$$

The water evaporation rate $S_m$, water-energy rate $S_{we}$, and air heat rate $S_{ae}$ equations [18, 25] are mentioned in Eq. (16), Eq. (17), and Eq. (18), respectively.

$$S_m = K_a\left(\frac{p_v^{"}}{RT_w} - \frac{p_v}{RT}\right)M_w \tag{16}$$

$$S_{we} = K_h(T_w - T) + S_m r_w \tag{17}$$

$$S_{ae} = K_h(T_w - T) + S_m c_{pv}(T_w - T) \tag{18}$$

These are the saturated vapor pressure $p_v^{"}$, the partial pressure of vapor $p_v$, the universal gas constant *R*, the droplet temperature $T_w$, the air temperature *T*, the molecular weight of droplet $M_w$, the latent heat of droplet $r_w$, and the specific heat of droplet at constant pressure $c_{pv}$.

*E. Interaction of air-water in fill*

Fill is an area where it extends contact between water and air, and because the flow of water is so complex that the formulation for this zone is an empirical equation from the experimental results. Usually recommended one is Merkel's method [15, 18, 26] to get the mass transfer coefficient $K_a$

$$K_a = B g_a^m Q^n \tag{19}$$

These are the experimental coefficients that are *B*, *m*, and *n*. Meanwhile, $g_a$ and *Q* are air velocity and capacity, respectively. The values of the coefficients depend on the width of the S-wave used. For 1.5 m widths, the values of 1.48, 0.69, and 0.3 are for *B*, *m*, and *n*, respectively. As for the width of 1.25 m, the values of 1.8639, 0.60, and 0.34 are for *B*, *m*, and *n*, respectively.

The water evaporation rate $S_m$ equation [18, 26] is

$$S_m = K_a\left(x_w^{"} - x_a\right) \tag{20}$$

These are the ratio of the humidity of moist air in saturated condition $x_w^{"}$ that is $x_w^{"} = 0.622p_v^{"}/\left(p - p_v^{"}\right)$ at water temperature $T_w$, the ratio of the humidity of moist air in ambient $x_a$ that is $x_a = \omega_v/(1 - \omega_v)$, and the fraction of the vapor mass $\omega_v$.

The heat transfer coefficient in volumetric $K_h$ [18, 26] is calculated by

$$K_h = K_a \cdot Le_f \tag{21}$$

The Lewis factor $Le_f$ is given by the Bošnjaković formula [27] that is

$$Le_f = 0.865^{2/3}\left[\left(\frac{x_w^{"}+j}{x_a+j} - 1\right)\Big/ ln\left(\frac{x_w^{"}+j}{x_a+j}\right)\right] \tag{22}$$

The ratio between $Le_f$ and *j* is assumed constant at 0.865 and, the ratio *j* between the molecular weight of water and air is 0.622. The water-energy rate $S_{we}$ and the air heat rate $S_{ae}$ equations in this zone are as same as in the other zones.

*F. Parameter's Measurement*

From the energy balance equation, assuming the Lewis number is 1 [28], an equation is obtained to estimate the change in droplet temperature as

$$\frac{dT_w}{dz} = \frac{6h_m}{c_{pv}\rho_w u_{wz} d}(r_{mw} - r_m) \tag{23}$$

The following are the enthalpy of saturated water $r_{mw}$, humid air $r_m$, and vapor $r_v$ [28] as in Eq. (24), Eq. (25), and Eq. (26), respectively.

$$r_{mw} = c_{pv}T_w + x_w^{"} r_v \tag{24}$$

$$r_m = c_p T + x_a\left(r_{w0} - c_{pv}T\right) \tag{25}$$

$$r_v = r_{w0} + c_{pv}T_w \tag{26}$$

These are the specific heat of air at constant pressure $c_p$, the enthalpy of water at 0°C $r_{w0}$, and the temperature of air *T*.

The process of mass transfer causes droplet mass to decrease when traversing. To get the mass difference equation, it is derived from the mass balance equation by combining the velocity [28] so

$$\frac{dm_w}{dz} = \rho_w \frac{\pi d^2}{2} \frac{d(d)}{dz} \quad (27)$$

where the diameter difference [28] along the tower is

$$\frac{d(d)}{dz} = \frac{2h_m(x_w^{"} - x_a)}{\rho_w u_{wz}} \quad (28)$$

Meanwhile, the humidity ratio equation along with the height of the tower was derived from the mass balance equation [28] as

$$\frac{d\omega_a}{dz} = \left(\frac{m_w}{m_a}\right) \frac{6h_m(x_w^{"} - x_a)}{\rho_w u_{wz} d} \quad (29)$$

Calculation of cooling tower effectiveness $\varepsilon$ [29] is the same as the calculation of heat exchanger performance as

$$\varepsilon = \frac{T_{w,i} - T_{w,o}}{T_{w,i} - T_{wb,i}} \quad (30)$$

These are the temperature of inlet water $T_{w,i}$, the temperature of outlet water $T_{w,o}$, and the temperature of the wet-bulb $T_{wb,i}$.

## IV. Results and Discussions

Before this study discusses the calculation results, it is needed to return to the purpose, which is to investigate the droplet heating process in the cooling tower. In the heating process, heat and mass transfer occurs in the droplets, which are the main study in this discussion. Therefore, all graphs were based on the droplet trajectory axis (*z*-axis), which had a starting point ($z = 0$) at the nozzle outlets and an endpoint ($z = H$) on the water surface in the water collector.

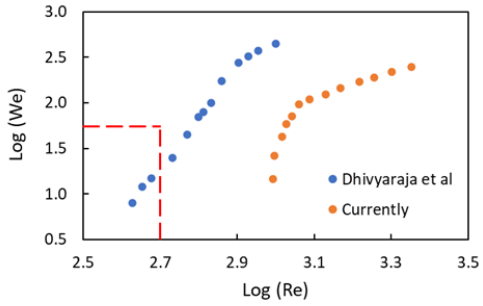


Fig. 3. Comparison of Re and We numbers.

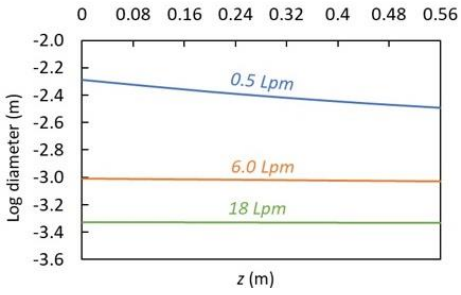


Fig. 4. The diameter of the droplet.

This study compared the dimensionless numbers from the experiment that it was being currently done to the attempt conducted by [2]. They used a nozzle 1 mm in diameter and were the same as the experiment this study was currently doing. The results of this comparison were presented in logarithms, as shown in Fig. 3.

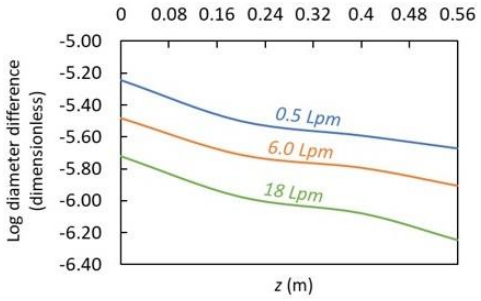


Fig. 5. The diameter reduction of the droplet.

The capacity of water through the nozzle strongly influenced the formulation of the Reynold and Weber numbers. The greater the water capacity, the greater the Reynold and Weber number. The capacity limit of our flowmeter was only up to 0.5 Lpm and could not read for lower capacities. Therefore, this study was in a turbulent region only in contrast to that of Dhivyaraja et al. [2] did it where it was in two zones, laminar (inside the red dotted line) and turbulent. It caused our Reynold and Weber number results to be larger than them.

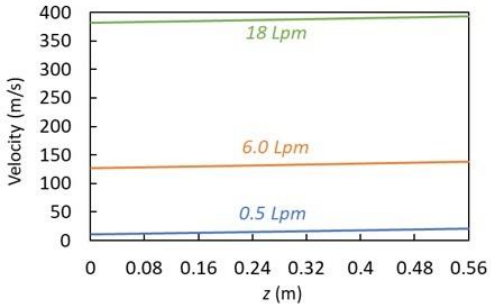


Fig. 6. The velocity of the droplet.

The diameter and diameter reduction along with the tower are discussed first because the diameter is directly related to the process of mass and heat transfer. As shown in Fig. 4, low capacity tends to have a large diameter, contrary to the high one tends to have a small diameter. The large diameter has a large surface area that facilitates the diffusion process between droplets and air, causing windage or water loss. The windage process is the same as the mass transfer because a lot of water is carried by exit air in the form of a liquid phase.

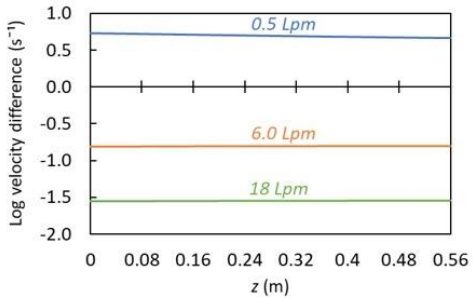


Fig. 7. The velocity reduction of the droplet.

Graphs in Fig. 5 are the result of the derivation of Fig. 4 where the lowest capacity gives the highest reduction. For the

high one, the graph appears constant because of the diameter reduction getting lower.

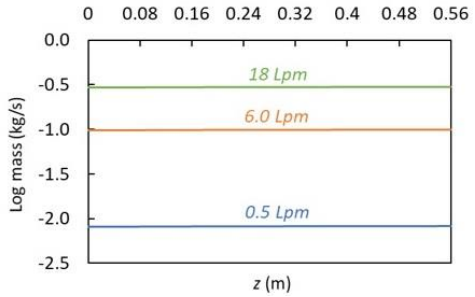


Fig. 8. Droplet mass flow.

Droplet velocity along the tower height is given by Fig. 6. High capacity provides high speed for the same cross-sectional area, which is the principle of continuity. Gravity has a small effect on velocity because of the high initial speed. It was obtained from the spraying process. In Fig. 7, overall velocity reduction is of small value because the influence of the upward moving air drag force is also relatively small compared to the initial droplet velocity.

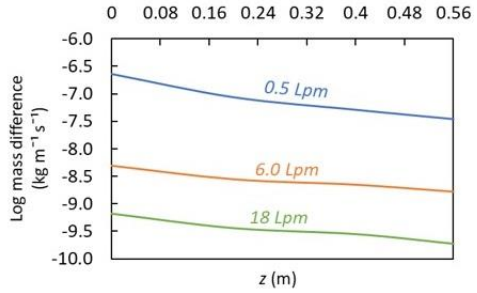


Fig. 9. Droplet mass flow reduction.

An interesting phenomenon is given by droplet mass flow graphs, as shown in Fig. 8 and the mass flow reduction graphs in Fig. 9. The lowest capacity has the smallest mass flow, while the reduction graph shows the highest value. It indicates that some droplet masses which were carried by air as losses. Towards the bottom of the tower, the reduction gets lower, which represents the mass loss in this section is lower than in the tower roof. It is possible because the air velocity at the bottom is lower than on the ceiling.

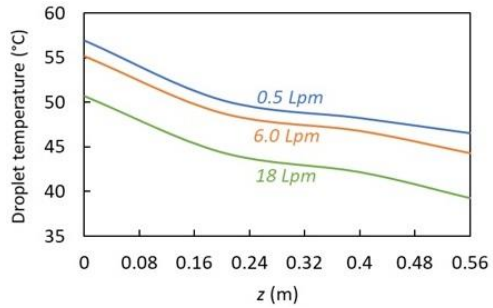


Fig. 10. Droplet temperature.

The opposite of the mass phenomenon occurs in droplet temperature graphs, as described in Fig. 10, and temperature reduction graphs, as figured in Fig. 11. This cooling tower is part of the system for heat dissipation so that the inlet temperature of the cooling tower varies. The intake temperature tends to be high for high capacities because the mass flow rate that carries heat is also high, whereas the low one is the opposite. The highest capacity has the lowest temperature, whereas the temperature reduction is highest. It denotes a high performance of heat transfer, which causes the highest reduction of the droplet temperature. The heat transfer is comparable to the degradation in it. The higher the degradation, the greater the heat transfer.

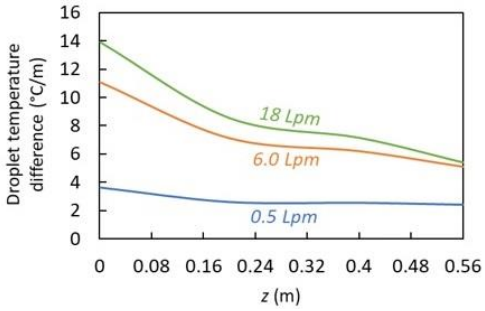


Fig. 11. Droplet temperature reduction.

In line with the droplet temperature, humidity graphs, as seen in Fig. 12, and humidity reduction graphs, as found in Fig. 13, have the same phenomenon. The highest capacity has the lowest humidity, which means that the water content in the air at that time was little, and most of the water has turned into steam. It results in the highest humidity reduction for the highest one, as shown in Fig. 13.

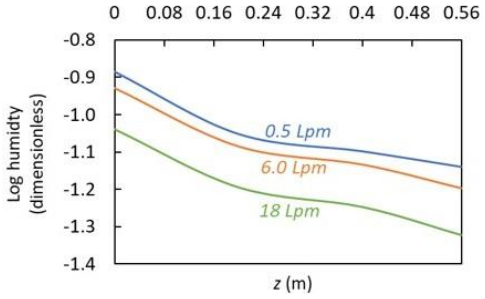


Fig. 12. Humidity.

The proof of all the discussion above is summarized in the performance graphs, as shown in Fig. 14. The highest water capacity and the highest fan rotation produce the highest effectiveness, although there is a limit of ambient temperature, which prevents graphs from value 1.

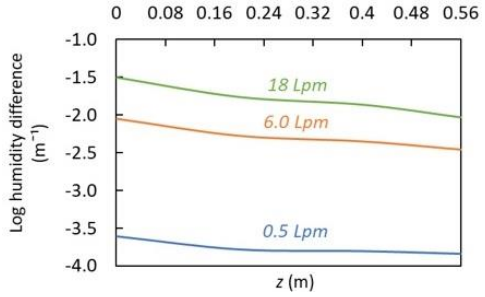


Fig. 13. Humidity reduction.

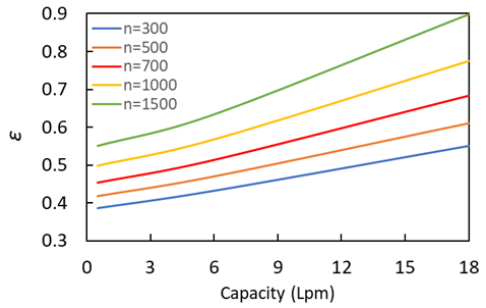


Fig. 14. The cooling tower effectiveness.

## CONCLUSIONS

For a capacity of 0.5 Lpm, the diameter had decreased due to the influence of the drag force. However, it cannot be immediately assumed that this reduction in diameter represented a reduction in mass. If it was compared with the mass flow reduction graph, for a capacity of 0.5 Lpm, there was a reduction in this along the path. It also happened for other ones but at a lower value. From this graph, it can be concluded that in all water capacities, there was a reduction in mass due to the influence of the drag force of the air flowing upwards. However, for a load of 18 Lpm, the mass reduction was smaller than for a capacity of 0.5 Lpm.

For a capacity of 18 Lpm, the temperature had the largest decrease, and the temperature reduction graph reinforced this, which showed the highest reduction value. From this information, it cannot be avoided that a high-temperature difference indicates a high heat transfer. Therefore, it can be concluded that heat and mass transfer processes occur in the droplet heating process. But it can be chosen which was more dominant between these by applying low or high capacity.

## REFERENCES


[1] A. Afzalifar, T. Turunen-Saaresti, A. Grönman, "Comparison of Moment-Based Methods for Representing Droplet Size Distributions in Supersonic Nucleating Flows of Steam," *Journal of Fluids Engineering*, vol. 140, no. 2, pp. 021301, Mar. 2017.

[2] K. Dhivyaraja, D. Gaddes, E. Freeman, S. Tadigadapa, M. V. Dynamical similarity and universality of drop size and velocity spectra in sprays," *Journal Fluid Mechanics*, vol. 860, pp. 510–543, 2019.

[3] J. A. L. Franca, J. P. A. R. da Cunha, U. R. Antuniassi, "Spectrum and velocity of droplet of spray nozzles with and without air induction," *Engenharia Agricola*, vol. 38, no. 2, pp. 232–237, 2018.

[4] Y. Akkus, Z. Dursunkaya, B. Çetin, "An Iterative Solution Approach to Coupled Heat and Mass Transfer in a Steadily Fed Evaporating Water Droplet," *Journal of Heat Transfer*, vol. 141, no. 3, pp. 031501, 2019.

[5] M. Zunaid, Q. Murtaza, S. Gautam, "Energy and performance analysis of multi droplets shower cooling tower at different inlet water temperature for air cooling application," *Applied Thermal Engineering*, vol. 121, pp. 1070–1079, 2017.

[6] S. S. Sazhin, "Modelling of fuel droplet heating and evaporation: Recent results and unsolved problems," *Fuel*, vol. 196, pp. 69–101, 2017.

[7] P. A. Strizhak, R. S. Volkov, G. Castanet, F. Lemoine, O. Rybdylova, S. S. Sazhin, "Heating and evaporation of suspended water droplets: Experimental studies and modelling," *International Journal of Heat and Mass Transfer*, vol. 127, pp. 92–106, 2018.

[8] G. V. Kuznetsov, P. A. Strizhak, R. S. Volkov, "Heat exchange of an evaporating droplet in a high-temperature environment," *International Journal of Thermal Sciences*, vol. 150, pp. 106227, 2020.

[9] G. V. Kuznetsov, M. V. Piskunov, R. S. Volkov, P. A. Strizhak, "Unsteady temperature fields of evaporating water droplets exposed to conductive, convective and radiative heating," *Applied Thermal Engineering*, vol. 131, pp. 340 – 355, 2018.

[10] T. Poós, V. Szabó, "Volumetric heat transfer coefficient in fluidized bed dryers," *Chemical Engineering & Technology*, vol. 41, no. 3, pp. 628 – 636, 2018.

[11] R. Petříček, T. Moucha, F. J. Rejl, L. Valenz, J. Haidl, T. Čmelíková, "Volumetric mass transfer coefficient, power input and gas hold-up in viscous liquid in mechanically agitated fermenters. Measurements and scale-up," *International Journal of Heat and Mass Transfer*, vol. 124, pp. 1117 – 1135, 2018.

[12] D. I. Santoso, B. Antoko, Prabowo, D. Ichsani, "Study of the evaporation process in the spray zone on a mechanical draft wet cooling tower," *Journal of Engineering and Technological Sciences*, vol. 53, no. 1, pp. 210204, 2021.

[13] L. Chen, X. Huang, L. Yang, X. Du, Y. Yang, "Evaluation of natural draft dry cooling system incorporating water spray air precooling," *Applied Thermal Engineering*, vol. 151, pp. 294–307, 2019.

[14] X. Huang, L. Chen, L., Yang, X. Du, Y. Yang, "Evaporation aided improvement for cooling performance of large-scale natural draft dry cooling system," *Applied Thermal Engineering*, vol 163, pp. 114350, 2019.

[15] H-W. Li, K-B. Wu, S-B. Wang, "Numerical simulation of the influence of flue gas discharge patterns on a natural draft wet cooling tower with flue gas injection," *Applied Thermal Engineering*, vol. 161, pp. 114137, 2019.

[16] M. Wang, J. Wang, J., Wang, C. Shi, "Contrastive Analysis of Cooling Performance between a High-Level Water Collecting Cooling Tower and a Typical Cooling Tower," *Journal of Thermal Science*, vol. 27, no. 1, pp. 39–47, 2018.

[17] Y. Zhao, F Sun, G. Long, X. Huang, W. Huang, D. Lyu, "Comparative study on the cooling characteristics of high-level water collecting natural draft wet cooling tower and the usual cooling tower," *Energy Conversion and Management*, vol. 116, pp. 150–164, 2016.

[18] D. Lyu, F. Sun, Y. Zhao, "Impact mechanism of different fill layout patterns on the cooling performance of the wet cooling tower with water collecting devices," *Applied Thermal Engineering*, vol. 110, pp. 1389–1400, 2017.

[19] B. Antoko, D. I. Santoso, A. B. K. Putra, Sutardi, "A study of air velocity in a cooling tower that affects the diameter of the droplet," *Journal of Mechanical Engineering*, vol. 18, no. 1, pp. 73–87, 2021.

[20] X. Chen, F. Sun, Y. Chen, M. Gao, "Novel method for improving the cooling performance of natural draft wet cooling towers," *Applied Thermal Engineering*, vol. 147, pp. 562–570, 2019.

[21] O. J. G. Pedraza, J. J. P. Ibarra, C. Rubio-Maya, S. R. G. González, J. A. R. Arista, "Numerical study of the drift and evaporation of water droplets cooled down by a forced stream of air," *Applied Thermal Engineering*, vol. 142, pp. 292–302, 2018.

[22] R. Onishi, K. Matsuda, and K. Takahashi, "Lagrangian tracking simulation of droplet growth in turbulence–turbulence enhancement of autoconversion rate," *Journal of the Atmospheric Sciences*, vol. 72, pp. 2591–2607, 2015.

[23] S. Kooij, R. Sijs, M. M. Denn, E. Villermaux, and D. Bonn, "What determines the drop size in sprays?" *Physical Review X*, vol. 8, pp. 031019, 2018.

[24] X. Chen, F. Sun, F., D. Lyu, "Field test study on water droplet diameter distribution in the rain zone of a natural draft wet cooling tower," *Applied Thermal Engineering*, vol. 162, pp. 114252, 2019.

[25] G. Chen, Y. Zhao, W. Ge, W. Li, "Critical guidelines to cope with the adverse impacts of the inner peripheral vortex in the high-level water collecting natural draft wet cooling tower," *Applied Thermal Engineering*, vol. 168, pp. 114819, 2020.

[26] R. S. Volkov, P. A. Strizhak, "Research of temperature fields and convection velocities in evaporating water droplets using Planar Laser-Induced Fluorescence and Particle Image Velocimetry," *Experimental Thermal and Fluid Science*, vol. 97, pp. 392–407, 2018.

[27] G. Chen, Y. Zhao, W. Li, W. Ge, "The efficiency of high-level water collecting cooling tower with the installation of cross wall affect by the evolution of aerodynamic field," *Applied Thermal Engineering*, vol. 161, pp. 114181, 2019.

[28] N. Gilani, A. D. Hendijani, R. Shirmohammadi, "Developing of a novel water-efficient configuration for shower cooling tower integrated with the liquid desiccant cooling system," *Applied Thermal Engineering*, vol. 154, pp. 180–195, 2019.

[29] X. Wei, N. Li, J. Peng, J. Hu, M. Wang, “Performance analyses of counter-flow closed wet cooling towers based on a simplified calculation method,” *Energies*, vol. 10, no. 3, pp. 282, 2017.